Acta Mechanica Sinica (2013) 29(5):649–656
DOI 10.1007/s10409-013-0079-1

RESEARCH PAPER

The effect of the couple stress parameter and Prandtl number on the transient natural convection flow over a vertical cylinder

H. P. Rani · G. Janardhana Reddy · Chang Nyung Kim

Received: 1 February 2013 / Revised: 18 July 2013 / Accepted: 5 September 2013

Abstract An analysis is performed to study transient free convective boundary layer flow of a couple stress fluid over a vertical cylinder, in the absence of body couples. The solution of the time-dependent non-linear and coupled governing equations is carried out with the aid of an unconditionally stable Crank–Nicolson type of numerical scheme. Numerical results for the steady-state velocity, temperature as well as the time histories of the skin-friction coefficient and Nusselt number are presented graphically and discussed. It is seen that for all flow variables as the couple stress control parameter, Co, is amplified, the time required for reaching the temporal maximum increases but the steady-state decreases.

Keywords Couple stress fluid · Natural convection · Vertical cylinder · Finite difference method

1 Introduction

In many engineering applications, especially in the glass and polymer industries, hot filaments, which are considered as vertical cylinders, are cooled as they pass through the surrounding environment. Some of these natural convection flows related to the Newtonian fluid flows past vertical bodies especially cylinders are cited here. Similar problem was analysed by Minkowycz and Sparrow [1] using the non-similarity method and for arbitrary Prandtl number, Fujiii and Uehara [2] analyzed the local heat transfer results. Then Lee et al. [3] investigated the power-law variation in the wall temperature for natural convective laminar boundary layer flow along slender vertical cylinders and needles. While the above studies deal only with the steady flows, the transient natural convection flow past thin wires was studied by Dring and Gebhart [4]. Then Velusamy and Garg [5] studied the transient natural convection over heat-generating vertical cylinders of various thermal capacities and radii, with the emphasis on the rate of propagation of the leading edge effect. The behaviour of unsteady wake for the flow past an inline arrangement of square cylinders confined in a channel was paid attention by Patil and Tiwari [6]. Rani and Kim [7] investigated the temperature-dependent viscosity and thermal conductivity for the transient free convection flow over an isothermal vertical cylinder. Recently, Zakaria and Gamiel [8] studied both the linear and nonlinear stability conditions of a viscous falling film around a vertical moving cylinder.

With the growing importance of non-Newtonian fluids in modern technology and industries, the investigations on such fluids are desirable. Stokes [9] generalized the classical Newtonian model to include the effect of couple stresses in a way different from that of Eringen [10]. This is one among the several non-Newtonian fluid theories that are developed in the twentieth century. In his theory Stokes considered a body enclosing a volume without considering the microstructures of the infinitesimal fluid volume element. The set of all forces acting on an infinitesimal volume element is, in general, assumed to be equivalent to a single resultant force together with a resultant couple. The moment of the couple is assumed to be of non zero value. With this assumption Stokes has proposed the theory of couple stress fluids allowing for the sustenance of couple stresses in addition to the usual stresses. Also, in his theory, curvature twist rate tensor is proposed based on the pure kinematic aspects of rotation vector and couple stress is defined in terms of this

H. P. Rani · G. J. Reddy
Department of Mathematics,
National Institute of Technology,
Warangal-506004, AP, India

C. N. Kim (✉)
Department of Mechanical Engineering,
College of Advanced Technology
(Industrial Liaison Research Institute),
Kyung Hee University, Gyeonggi-do 446-701, Korea
e-mail: cnkim@khu.ac.kr

curvature twist rate tensor. Accordingly, in the balance of linear momentum of the couple stress flow model, fourth order derivatives of velocities are involved and, hence, separate angular momentum equation need not be considered. These fluids can also sustain the existence of body forces as usual and in addition by body couples as well. The stress tensor is no longer symmetric in this theory. The fluids consisting of rigid, randomly oriented particles suspended in a viscous medium, such as blood, lubricants containing small amount of polymer additive, electro-rheological fluids and synthetic fluids are some of the examples for these couple stress fluids. This couple stress model has been widely used because of its great mathematical simplicity compared to that of the other models developed for the polar fluids. Recently, the study of couple stress fluid flows has been the subject of great interest, due to its widespread industrial and scientific applications as in the case of micropolar fluids. Important field where couple stress fluids have applications includes squeezing and lubrication [11–14], bio-fluidmechanics [15, 16], MHD flows and synthesis and plasticity of chemical compounds. Another interesting application was studied by Umavathi and Malashetty [17] for the flow and heat transfer characteristics of Oberbeck convection of a couple stress fluid in a vertical porous stratum. Srinivasacharya and Kaladhar [18] investigated the hall and ion-slip effects on fully developed electrically conducting couple stress fluid flow between vertical parallel plates in the presence of a temperature dependent heat source. Recently, Rani et al. [19] obtained the numerical solution for the transient free convective couple stress fluid flow past a vertical cylinder.

It can be noted, from the past studies, that the unsteady natural convection flow of a viscous incompressible couple stress fluid over a uniformly heated vertical cylinder has been paid very little attention. Hence, in the present study it is aimed to study the boundary layer region developed by a isothermal vertical cylinder, which is kept in a couple stress fluid. The surface temperature of the cylinder is considered to be higher than that of the ambient fluid temperature. The non-dimensional unsteady non-linear partial differential equations which govern the momentum and heat transfer are solved numerically with the help of Thomas and pentadiagonal algorithms. The transient effects of the couple stress fluid based on the flow profiles with time for different non-dimensional numbers are analyzed and compared with those of the Newtonian fluids.

2 Mathematical modelling

A couple stress viscous incompressible fluid flow over a uniformly heated semi-infinite vertical cylinder of radius r_0 is considered as shown in Fig. 1. The axial (x) and radial (r) coordinates of the cylinder are measured vertically upward and perpendicular to the axis, respectively, from the leading edge where the boundary layer thickness is zero. The surrounding stationary fluid temperature is assumed to be of ambient temperature, say, T'_∞. Initially, i.e., at time $t' = 0$, it is assumed that the cylinder and the fluid are of the same temperature, T'_∞. As time increases ($t' > 0$), the temperature of the cylinder is amplified to $T'_w (> T'_\infty)$ and is kept constant there afterwards. It is assumed that the effect of viscous dissipation is negligible in the energy equation since the flow velocity magnitude is expected to be small.

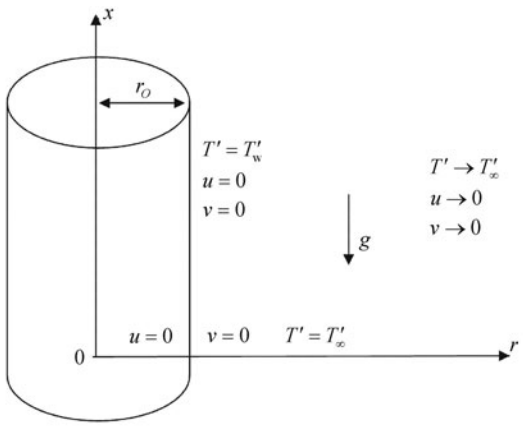

Fig. 1 Physical model and coordinate system

2.1 Governing equations

Based on the above assumptions and Boussinesq's approximation, the flow of an incompressible couple stress fluid in the absence of body couple, the boundary layer equations along with the energy equation are as follows:

(1) Conservation of mass

$$\frac{\partial(ru)}{\partial x} + \frac{\partial(rv)}{\partial r} = 0; \tag{1}$$

(2) Conservation of momentum

$$\rho\left(\frac{\partial u}{\partial t'} + u\frac{\partial u}{\partial x} + v\frac{\partial u}{\partial r}\right) = \rho g \beta_T \left(T' - T_\infty{}'\right) + \frac{1}{r}\frac{\partial}{\partial r}\left(\mu r \frac{\partial u}{\partial r}\right) - \eta \nabla^4 u; \tag{2}$$

(3) Energy equation

$$\frac{\partial T'}{\partial t'} + u\frac{\partial T'}{\partial x} + v\frac{\partial T'}{\partial r} = \frac{\alpha}{r}\frac{\partial}{\partial r}\left(r\frac{\partial T'}{\partial r}\right), \tag{3}$$

where u and v are the velocity components parallel to x and r coordinates, respectively, g is the acceleration due to gravity, β_T is the volumetric coefficient of thermal expansion, ρ is the density and α is the thermal diffusivity.

The constitutive equations concerning the force stress tensor t_{ij} and the couple stress tensor m_{ij} that arises in the theory of couple stress fluids are given by [9]

$$t_{ij} = (-p + \lambda \nabla \cdot \boldsymbol{U})\delta_{ij} + 2\mu d_{ij} - \frac{1}{2}\varepsilon_{ijk}(m_{,k} + 4\eta\omega_{k,rr} + \rho c_k), \tag{4}$$

$$m_{ij} = \frac{1}{3} m \delta_{ij} + 4\eta' \omega_{j,i} + 4\eta \omega_{i,j}. \tag{5}$$

In the above Eqs. (4)–(5), $\boldsymbol{U}$ is the velocity vector, $\boldsymbol{\omega}(= \frac{1}{2}\nabla \times \boldsymbol{U})$ is the spin vector, $\omega_{i,j}$ is the spin tensor, d_{ij} is the rate of deformation tensor, $m(= m_{11} + m_{22} + m_{33})$ is the trace of the couple stress tensor m_{ij}, p is the fluid pressure, δ_{ij} is the kronecker delta, ε_{ijk} is the Levi–Civita symbol and ρc_k is the body couple vector. Comma in the suffixes denotes covariant differentiation and $\omega_{k,rr}$ stands for $\omega_{k,11}+\omega_{k,22}+\omega_{k,33}$.

The quantities λ and μ are the viscosity coefficients and η, η' are the couple stress viscosity coefficients. These material constants are constrained by the following inequalities as

$$\mu \geqslant 0, \quad 3\lambda + 2\mu \geqslant 0, \quad \eta \geqslant 0, \quad |\eta'| \leqslant \eta. \tag{6}$$

The corresponding initial and boundary conditions are given by

$$\begin{aligned}
&t' = 0: \ u = 0, \quad v = 0, \quad T' = T'_\infty, && \text{for all } x \text{ and } r,\\
&t' > 0: \ u = 0, \quad v = 0, \quad T' = T'_w, && \text{at } r = r_0,\\
&\qquad\ u = 0, \quad v = 0, \quad T' = T'_\infty, && \text{at } x = 0,\\
&\qquad\ u \to 0, \quad v \to 0, \quad T' \to T'_\infty, && \text{as } r \to \infty.
\end{aligned} \tag{7}$$

It can be noted that for couple stress fluids, the vorticity of the fluid on the boundary is equal to the rotational velocity of the boundary [20], i.e., Curl $\boldsymbol{U} = 0 \Rightarrow \dfrac{\partial u}{\partial r} = \dfrac{\partial v}{\partial x}$ at $r = r_0$ and as $r \to \infty$.

Now, the following non-dimensional quantities are introduced

$$\begin{aligned}
&X = Gr_T^{-1}\frac{x}{r_0}, && R = \frac{r}{r_0},\\
&U = Gr_T^{-1}\frac{ur_0}{\nu}, && V = \frac{vr_0}{\nu},\\
&t = \frac{\nu t'}{r_0^2}, && T = \frac{T' - T_\infty{}'}{T_w{}' - T_\infty{}'},\\
&Gr_T = \frac{g\beta_T r_0^3 (T'_w - T'_\infty)}{\nu^2}, && Pr = \frac{\nu}{\alpha},\\
&Co = \frac{\eta}{\mu r_0^2},
\end{aligned} \tag{8}$$

where ν is the reference kinematic viscosity, Gr_T, Pr, and Co denote the Grashof number, the Prandtl number, and the couple stress parameter, respectively.

By introducing the above non-dimensional quantities into the Eqs. (1)–(3), they are reduced to the following form

$$\frac{\partial U}{\partial X} + \frac{\partial V}{\partial R} + \frac{V}{R} = 0, \tag{9}$$

$$\frac{\partial U}{\partial t} + U\frac{\partial U}{\partial X} + V\frac{\partial U}{\partial R} = T + \left(\frac{\partial^2 U}{\partial R^2} + \frac{1}{R}\frac{\partial U}{\partial R}\right) - Co\left(\frac{1}{R^3}\frac{\partial U}{\partial R} - \frac{1}{R^2}\frac{\partial^2 U}{\partial R^2} + \frac{2}{R}\frac{\partial^3 U}{\partial R^3} + \frac{\partial^4 U}{\partial R^4}\right), \tag{10}$$

$$\frac{\partial T}{\partial t} + U\frac{\partial T}{\partial X} + V\frac{\partial T}{\partial R} = \frac{1}{Pr}\left(\frac{\partial^2 T}{\partial R^2} + \frac{1}{R}\frac{\partial T}{\partial R}\right) \tag{11}$$

with initial and boundary conditions

$$\begin{aligned}
&t = 0: \ U = 0, \quad V = 0, \quad T = 0, && \text{for all } X \text{ and } R,\\
&t > 0: \ U = 0, \quad V = 0, \quad T = 1, && \text{at } R = 1,\\
&\qquad\ U = 0, \quad V = 0, \quad T = 0, && \text{at } X = 0,\\
&\qquad\ U \to 0, \quad V \to 0, \quad T \to 0, && \text{as } R \to \infty.
\end{aligned} \tag{12}$$

$$\frac{\partial U}{\partial R} = \frac{1}{Gr_T^2}\frac{\partial V}{\partial X}, \quad \text{at } R = 1 \text{ and as } R \to \infty.$$

In order to solve the unsteady coupled non-linear governing Eqs. (9)–(11) an implicit finite difference scheme of Crank–Nicolson type has been employed. The region of integration is considered as a rectangle composed of the lines indicating $X_{\min} = 0$, $X_{\max} = 1$, $R_{\min} = 1$, and $R_{\max} = 20$, where $R_{\max}$ corresponds to $R = \infty$ which lies very far from the momentum and energy boundary layers. The mesh density has been varied so that the computed solutions represent the real flow physics. A series of grid independence tests was conducted to determine the optimal mesh. The steady-state velocity and temperature values obtained with the grid system of 100×500 differ in the second decimal place from those with the grid system of 50×250, and in the fifth decimal place from those with the grid system of $200 \times 1\,000$. Hence, in the present analysis, for more accurate results, which is close to the physically meaning full results, the fine grid size 100×500 was selected as the optimal mesh for all subsequent analyses, with mesh size in X and R direction are taken as 0.01 and 0.038, respectively. Also, the time step size dependency has been carried out, from which 0.01 yielded a reliable result. The steady-state solution is assumed to have been reached when the absolute difference between the values of velocity as well as temperature at two consecutive time steps is less than 10^{-5} at all grid points.

3 Results and discussion

To corroborate the current numerical procedure, the profiles of simulated flow variables for the case of Newtonian fluids ($Co = 0.0$) are compared with those of the steady-state isothermal results of Lee et al. [3]. The comparison results, which are shown in Fig. 2, are found to be in good agreement. These results substantiate the validity and accuracy of the present numerical solution.

The simulated results are presented to outline the general physics for different values of control parameters, Pr (= 0.7 (gases), 7.0 (molten salts), and 30.0 (inorganic liquids)) [21] and Co (= 0.0, 1.0 and 3.0). The simulated transient behaviour of the dimensionless velocity, temperature and average skin-friction and heat transfer coefficients are discussed in detail in the succeeding subsections.

3.1 Flow variables

To analyze the transient behavior of the simulated flow variables, such as velocity and temperature, their values are depicted at different locations, which are close and distant to

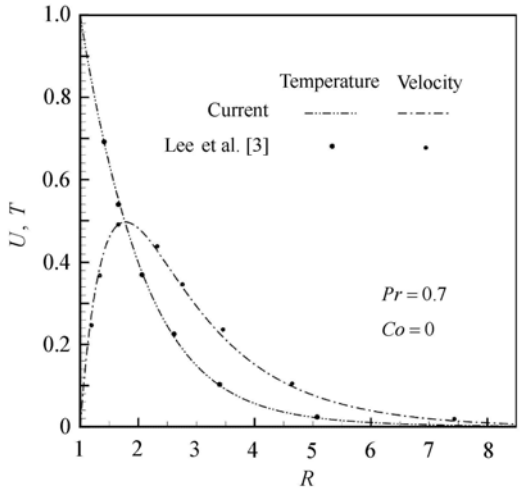

Fig. 2 Comparison of the velocity and temperature profiles with Lee et al. [3]

the cylinder wall. The steady-state velocity and temperature profiles are shown against the radial coordinate at $X = 1.0$. The above details are discussed with respect to the control parameters and their behavior is discussed. It is observed that the time taken to reach the steady-state increases with augmenting Pr or decreasing Co. It is observed that the convection contribution initially increases with time, attains the temporal maximum and subsequently reaches the steady-state asymptotically.

3.1.1 Velocity

The obtained transient dimensionless velocity (U) profiles at two different locations, namely, (1, 2.98) and (1, 4.5) for different Pr and Co are graphically represented in Fig. 3 against the time, t. Figures 3a and 3b represent the velocity profiles that are considered at the proximity and distant from the hot wall, respectively. It is observed that at all the locations the velocity increases with time, reaches a temporal maximum, then decreases and at last reaches the asymptotic steady-state. For example for the case of couple stress fluids ($Co > 0$) and $Pr = 7$, the wall velocity upsurges with time monotonically, reaches the temporal maximum, then slightly decreases and at last becomes asymptotically steady. It is observed that in the early hours (i.e., $t \ll 1$), the heat transfer is dominated by conduction. Shortly later, there exists a period where the heat transfer rate is influenced by the effect of convection with the increasing upward velocities. Prior to the end of transient period or just before reaching the steady-state, there exist overshoots of the velocities. As noted in Figs. 3a and 3b, the magnitude of this overshoot of the velocities decreases as Pr is augmented, since the increasing Pr leads to the increase in size of the term of velocity diffusion (refer Eq. (10)) and there is a less resistance to the fluid flow in the region of the temporal maximum of velocity. The time required to reach the temporal maximum of the velocity and the steady-state increases with augmenting Pr. Also, as the couple stress control parameter, Co, is amplified, the time required for reaching the temporal maximum increases but the steady-state decreases. Similar trend is observed for the Newtonian fluids also. The transient characteristics of temperature that are similar to the velocity are detailed in Fig. 5 and will be discussed elsewhere. From Fig. 3a it is observed that when Pr is small (i.e., $Pr = 0.7$) the transient velocity values of the couple stress fluid is less than that of the Newtonian fluid but for increasing Pr (= 7, 30) this trend is opposite. While for all values of Pr the transient velocity of the couple stress fluid is greater than that of the Newtonian fluid as shown in Fig. 3b. This fluctuating behavior of velocity with respect to Pr will be justified with the aid of Fig. 4 in the succeeding paragraph.

Figure 4 shows the simulated steady-state velocity profiles against R at $X = 1.0$. From this figure it is observed that the velocity profile start with the no-slip value at the wall, reach their maximum and then monotonically decrease to zero along the radial coordinate for all values of t, thus satisfying the far-away boundary conditions. Also in the vicinity of the wall the magnitude of the axial velocity is rapidly

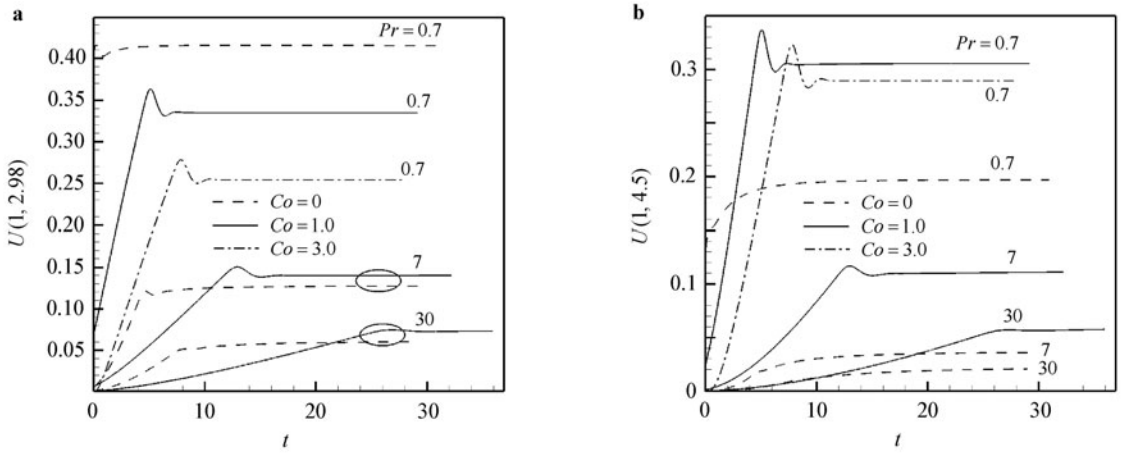

Fig. 3 The simulated transient velocity (U) against time (t) for different values of Pr and Co at the point: **a** (1, 2.98); **b** (1, 4.5)

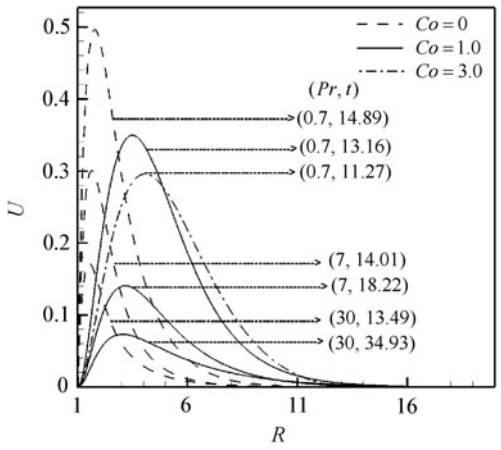

Fig. 4 The simulated steady-state velocity (U) profiles against R at $X = 1.0$ for different values of Pr and Co

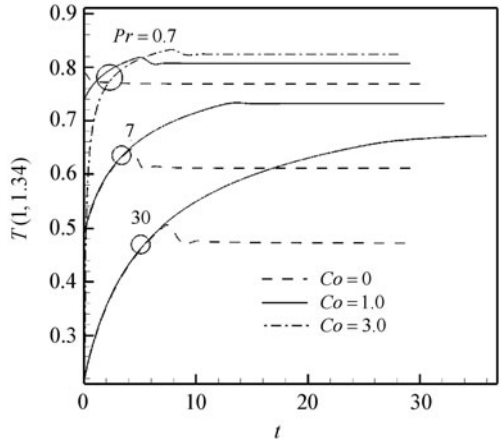

Fig. 5 The simulated transient temperature (T) against time (t) at the point (1, 1.34) for different values of Pr and Co

increasing as the radial coordinate grows from $R_{\min}$ (= 1). Also, it can be noted that the time to reach the steady-state increases with augmenting Pr or decreasing Co. The velocity decreases with the increasing Pr due to the fact that the effect of velocity diffusion gets increased for high values of Pr. When Pr is increased, the thermal convection is confined to a region near the hot wall, while the momentum diffusion is propagated far from the hot wall and hence the high velocity profiles are observed in the proximity of the hot wall. Similar decreasing trend of velocity profiles is observed for increasing values of Co.

The deviation of velocity profiles from the hot wall is more for the couple stress fluids in comparison with that of the Newtonian fluids. Also it can be observed that in the vicinity of hot wall the magnitude of velocity for the Newtonian fluids is higher than that of the couple stress fluids while far away from the hot wall this trend reverses. For example, when $Pr = 0.7$ the velocity profiles of the Newtonian fluids shows higher values than those of the couple stress fluids in the region, $1 < R < 3.6$ while the opposite trend is observed for $R > 3.6$. Similar observation is already noted in Figs. 3a and 3b. Thus, it can be concluded that the transient velocity profiles for the couple stress fluids flow differ from those of the Newtonian fluids flow.

3.1.2 Temperature

The obtained transient temperature profiles for different values of Pr and Co values are shown at the point (1, 1.34) against the time in Fig. 5. The oscillatory nature of the temperature profiles are observed until it reaches the steady-state values. The transient temperature profiles increase with time, reach a temporal maximum, decrease and again after slightly increasing attain the steady-state asymptotically. The temperature at other locations also exhibits somewhat similar transient behavior. During the initial period, the nature of the transient temperature profiles with respect to Pr is particularly noticeable. For the values of amplified Pr the transient temperature profiles of the couple stress fluid initially coincide with that of the Newtonian fluid and then get deviated after some time. For example, when $Pr = 7$ the transient temperature of a couple stress fluid deviates from that of the Newtonian fluid at time $t = 4.14$. As seen before, during the initial time period, the couple stress fluid follows the characteristics of Newtonian fluid for $Pr = 7$ and 30, but the concurrence period of the temperature profiles between the couple stress fluid and Newtonian fluid increases with the increasing Pr. Hence, it can be said that during the initial period the temperature profiles for both couple stress fluid and Newtonian fluid exhibit similar behavior. The time required for attaining the temporal maximum of the temperature demands the high values of Pr or Co. The maximum peak value of the temperature decreases with the increasing Pr and also as Pr increases the transient temperature values of the couple stress fluid is greater than that of the Newtonian fluid. It is also observed that for fixed values of Pr, as the Co amplifies the maximum peak temperature value increases.

The simulated steady-state temperature profiles at $X = 1.0$ against the R-coordinate are shown in Fig. 6 for different values of Pr and Co. The temperature profiles start with the hot wall temperature ($T = 1$) and then monotonically decrease to zero along the radial coordinate for all time. It is related to the fact that the effect of velocity diffusion gets increased for high Pr, which allows higher velocity in the vicinity of the hot wall. Also, for increasing Pr values the time taken to reach the steady-state increases. While for increasing Co the opposite trend is observed. The boundary layer becomes thicker as the values of Co increases. Larger Pr values give rise to thinner temperature profiles, since a larger Pr value means that the thermal diffusion from the wall is not prevailing while the velocity diffusion tries to move away from the wall. Also from Fig. 5 it is observed that the transient temperature profiles for the couple stress fluid differ from those of the Newtonian fluids. Similar observation is noticed in Fig. 6. Also it is observed that as Pr increases the deviation of the transient temperature profiles

from the hot wall for a couple stress fluid is much more than that of the Newtonian fluid. Thus, it can be concluded that the transient temperature profiles for the couple stress fluid differ from those of the Newtonian fluid.

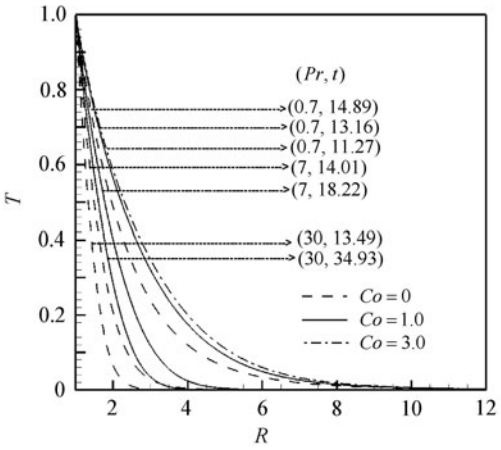

Fig. 6 The simulated steady-state temperature (T) profiles against R at $X = 1.0$ for different values of Pr and Co

3.2 Average momentum and heat transport coefficients

Knowing the unsteady behavior of velocity and temperature profiles from the solution of the Eqs. (9)–(11) along with the initial and boundary conditions Eq. (12), it is worth to study the average skin-friction coefficient and the average heat transfer rate (Nusselt number). The increased skin-friction is generally a handicap in many technical applications, while the increased heat transfer can be exploited in some applications such as heat exchangers, but should be avoided in others such as gas turbine applications, for instance. The non-dimensional average skin-friction coefficient and Nusselt number are given by $\overline{C_{\mathrm{f}}} = \int_0^1 \left(\frac{\partial U}{\partial R}\right)_{R=1} \mathrm{d}X$ and $\overline{Nu} = -\int_0^1 \left(\frac{\partial T}{\partial R}\right)_{R=1} \mathrm{d}X$, respectively. The derivatives are evaluated by using a five-point approximation formula and then the integrals are evaluated by using the Newton–Cotes closed integration formula. The simulated average non-dimensional skin friction and heat transfer coefficients for Newtonian and couple stress fluids have been plotted against the time in Figs. 7 and 8, respectively, for different Pr and Co values.

The effects of Pr and Co on the simulated average skin-friction coefficient ($\overline{C_{\mathrm{f}}}$) are shown in Fig. 7. From Fig. 7 it is observed that for all values of Pr and Co the $\overline{C_{\mathrm{f}}}$ increases with time, attains the maximum value and, after slightly decreasing, becomes asymptotically steady. It is also observed from Fig. 7 that for increasing values of Co or Pr the $\overline{C_{\mathrm{f}}}$ decreases. This result lies in the same line with the velocity profiles plotted in Fig. 4. In particular it is observed that as Pr increases the $\overline{C_{\mathrm{f}}}$ of a couple stress fluid is decreased in comparison with that of the Newtonian fluid.

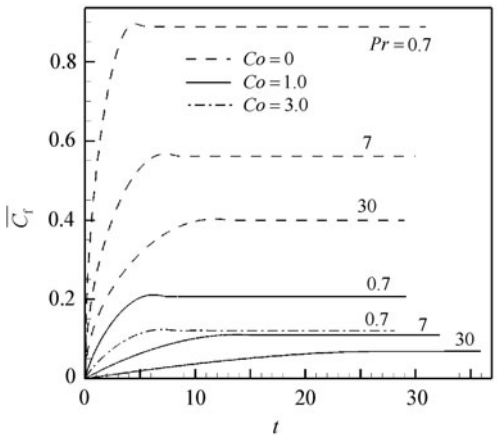

Fig. 7 The simulated average skin friction ($\overline{C_{\mathrm{f}}}$) for different values of Pr and Co

In Fig. 8 the effects of Pr and Co on the simulated average heat transfer rate ($\overline{Nu}$) are shown. Figure 8 reveals that an increase in the value of Pr leads to an increase in the values of the $\overline{Nu}$. Also as Pr increases the $\overline{Nu}$ of a couple stress fluid is decreased compared to that of the Newtonian fluid. Increasing Pr speeds up the spatial decay of the temperature field near the heated surface, yielding an increase in the rate of heat transfer. Also, for fixed Pr, the $\overline{Nu}$ decreases with the increasing values of Co. From Figs. 7 and 8 it is observed that the $\overline{C_{\mathrm{f}}}$ and $\overline{Nu}$ of a couple stress fluid differ from those of the Newtonian fluids.

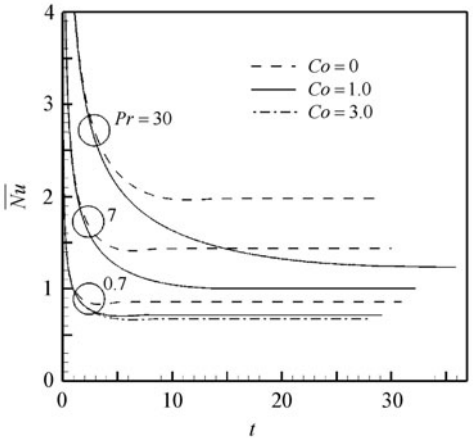

Fig. 8 The simulated average Nusselt number ($\overline{Nu}$) for different values of Pr and Co

3.3 Comparison between couple stress and Newtonian fluids

Figure 9 illustrates the steady-state U and T contours for couple stress and Newtonian fluid flows with fixed $Pr = 0.71$. It can be noticed that from Figs. 9a and 9b, the velocity of the couple stress fluid flow is much less compared to that of the Newtonian fluid flow, while the opposite trend is observed for the temperature. This is due to the fact that in

couple stress fluid flow there are additive diffusion terms (biharmonic term) compared with that of the Newtonian fluid flow (refer Eq. (10)). Also, from Figs. 9a and 9b it is observed that the steady-state temperature contours for the couple stress fluid are somewhat different, with thicker temperature layer, from those of the Newtonian fluid.

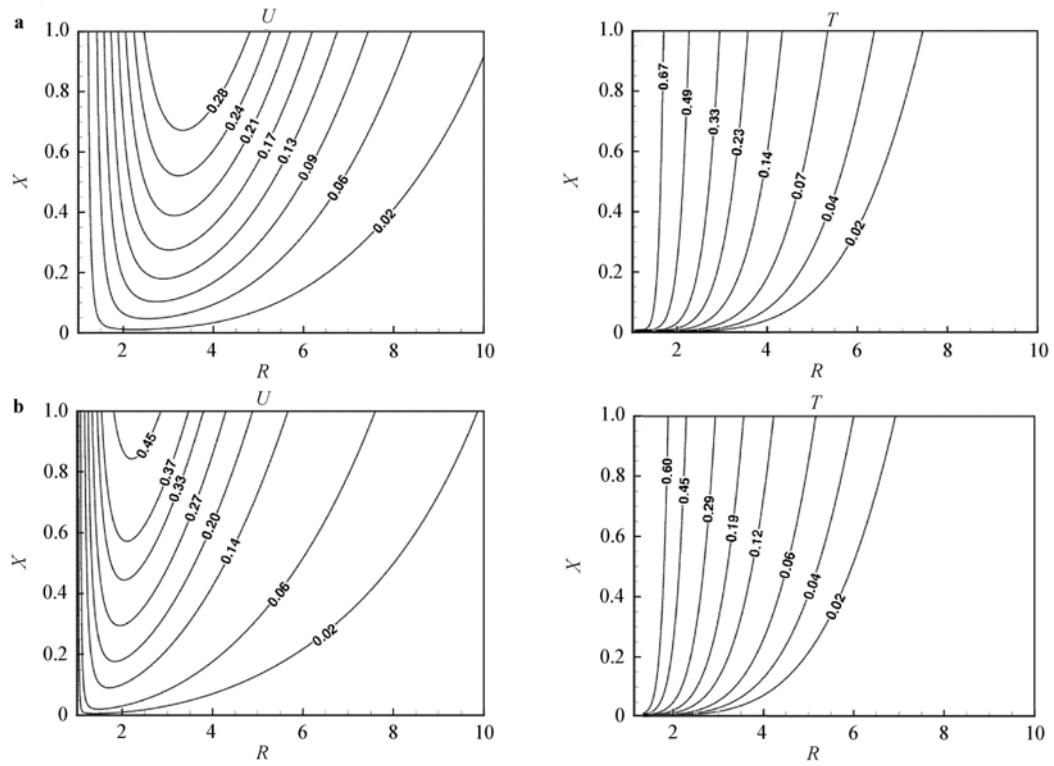

Fig. 9 Steady-state velocity (U) and temperature (T) contours with $Pr = 0.71$ for **a** couple stress fluid ($Co = 1.0$); **b** Newtonian fluid ($Co = 0.0$)

4 Conclusions

In this paper, the unsteady natural convective couple stress viscous incompressible fluid flows over a semi-infinite heated vertical cylinder are studied numerically. The governing equations are normalised based on the length dependent effect introduced by the couple stress fluid. A Crank-Nicolson type of implicit method is used to solve the governing unsteady, non-linear and coupled equations. The resulting system of equations is solved by using the Thomas and Pentadiagonal algorithms. The computations are carried out for different values of the Pr and couple stress parameter (Co). It is observed that the time elapsed for the velocity and temperature profiles to reach the steady-state increases with increasing Pr. While the reverse trend is observed for Co. For $Pr > 1$, initially, the unsteady behaviour of the flow characteristics for the couple stress fluid coincides with, then deviates from, that of the Newtonian fluid, and they reach the steady-state asymptotically. When $Pr < 1$, a higher velocity is observed in a region near the wall, and further increase in Pr leads to an increase in the average heat transfer rate and a decrease in the average skin-friction. As Pr increases both the average skin-friction coefficient and average heat transfer rate of a couple stress fluid are notably decreased compared to those of the Newtonian fluid. It is also noticed that as Co increases, both the average skin-friction and average heat transfer rate decrease. In couple stress fluid flow the deviation of the position of peak velocity for the transient flow from the hot wall is much more than that for the Newtonian fluid flow. Particularly, this study reveals that the results pertaining to the couple stress fluid differ significantly from those of the Newtonian fluid.

References

1 Minkowycz, W.J., Sparrow, E.M.: Local nonsimilar solutions for natural convection on a vertical cylinder. J. Heat Transfer **96**, 178–183 (1974)
2 Fujii, T., Uehara, H.: Laminar natural convective heat transfer from the outer surface of a vertical cylinder. Int. J. Heat Mass Transfer **13**, 607–615 (1970)
3 Lee, H.R., Chen, T.S., Armaly, B.F.: Natural convection along slender vertical cylinders with variable surface temperature. J. Heat Transfer **110**, 103–108 (1988)
4 Dring, R.P., Gebhart, B.: Transient natural convection from thin vertical cylinders. J. Heat Transfer **88**, 246–247 (1966)
5 Velusamy, K., Garg, V.K.: Transient natural convection over a heat generating vertical cylinder. Int. J. Heat Mass Transfer **35**,

1293–1306 (1992)
6 Patil, P.P., Tiwari, S.: Numerical investigation of laminar unsteady wakes behind two inline square cylinders confined in a channel. Eng. Appl. Comput. Fluid Mech. **3**, 369–385 (2009)
7 Rani, H.P., Kim, C.N.: Transient convection on a vertical cylinder with variable viscosity and thermal Conductivity. J. Thermophy. and Heat Transfer **22**, 254–261 (2008)
8 Zakaria, K., Gamiel, Y.: Viscous falling film instability around a vertical moving cylinder. Acta Mech. Sin. **28**, 253–265 (2012)
9 Stokes, V.K.: Couple stress in fluids. Phys. Fluids **9**, 1709–1715 (1966)
10 Eringen, A.C.: Theory of micropolar fluids. J. Math. Mech. **16**, 1–18 (1966)
11 Chu, H.M., Li, W.L., Hu, S.Y.: Effects of couple stresses on pure squeeze EHL motion of circular contacts. J. Mech. **22**, 77–84 (2006)
12 Lin, J.: Squeeze film characteristics of finite journal bearings: Couple stress fluid model. Tribology Int. **31**, 201–207 (1998)
13 Naduvinamani, N.B., Patil, S.B.: Numerical solution of finite modified Reynolds equation for couple stress squeeze film lubrication of porous journal bearings. Comput. Struct. **87**, 1287–1295 (2009)
14 Chang-Jian, C., Yau, H., Chen, J.: Nonlinear dynamic analysis of a hybrid squeeze-film damper-mounted rigid rotor lubricated with couple stress fluid and active control. Appl. Math. Modell. **34**, 2493–2507 (2010)
15 Srivastava, V.P.: Flow of a couple stress fluid representing blood through stenotic vessels with a peripheral layer. Indian J. Pure and Appl. Math. **34**, 1727–1740 (2003)
16 Srivastava, L.M.: Peristaltic transport of a couple stress fluid. Rheol Acta **25**, 638–641 (1986)
17 Umavathi, J.C., Malashetty, M.S.: Oberbeck convection flow of a couple stress fluid through a vertical porous stratum. Int. J. Non-Linear Mech. **34**, 1037–1045 (1999)
18 Srinivasacharya, D., Kaladhar, K.: Natural convection flow of a couple stress fluid between two vertical parallel plates with Hall and ion-slip effects. Acta Mech. Sin. **28**, 41–50 (2012)
19 Rani, H.P., Janardhana Reddy, G., Kim, C.N.: Numerical analysis of couple stress fluid past an infinite vertical cylinder. Eng. Appl. Comput. Fluid Mech. **5**, 159–169 (2011)
20 Stokes, V.K.: Theories of Fluids with Microstructure, Springer-Verlag, New York (1984)
21 Lappa, M.: Thermal Convection: Patterns, Evolution and Stability, John Wiley and Sons (2010)